ACS OMEGA

Open Access

http://pubs.acs.org/journal/acsodf

Article

Comprehensive Study on the Adsorption and Degradation of Dichlorodiphenyltrichloroethane on Bifunctional Adsorption−Photocatalysis Material TiO_2/MCM-41 Using Quantum Chemical Methods

Nguyen Thi Thu Ha, Hoang Lan Ngo, Thi Be Pham, Nguyen Hoang Hao, Cong Trinh Bui, Thi Lan Phung, Le Minh Cam, and Nguyen Ngoc Ha*

Cite This: *ACS Omega* 2024, 9, 7976−7985

Read Online

ACCESS | Metrics & More | Article Recommendations | Supporting Information

ABSTRACT: The adsorption and degradation capacities of dichlorodiphenyltrichloroethane (DDT) on a photocatalyst composed of TiO_2 supported on the mesoporous material MCM-41 (TiO_2/MCM-41) were investigated using density functional theory and real-time density functional theory methods. The van der Waals interactions within the PBE functional were adjusted by using the Grimme approach. The adsorption of DDT was evaluated through analyses involving adsorption energy, Hirshfeld atomic charges, Wiberg bond orders, molecular electrostatic potential, noncovalent interaction analysis, and bond path analysis. The findings reveal that DDT undergoes physical adsorption on pristine MCM-41 or MCM-41 modified with Al or Fe due to the very small bond order (only about 0.15−0.18) as well as the change in total charge of DDT after adsorption is close to 0. However, it chemically adsorbs onto the TiO_2/MCM-41 composite through the formation of Ti···Cl coordination bonds because the maximum bond order is very large, about 1.0 (it can be considered as a single bond). The adsorption process is significantly influenced by van der Waals interactions (accounting for approximately 30−40% of the interaction energy), hydrogen bonding, and halogen bonding. MCM-41 is demonstrated to concurrently function as a support for the TiO_2 photocatalyst, creating a synergistic effect that enhances the photocatalytic activity of TiO_2. Based on the computational results, a novel photocatalytic mechanism for the degradation of DDT on the TiO_2/MCM-41 catalyst system was proposed.

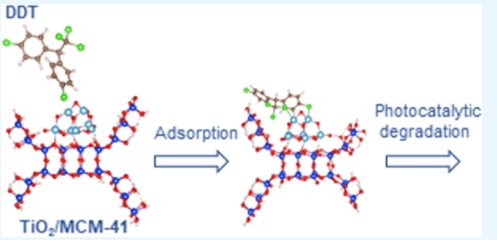

1. INTRODUCTION

DDT (1,1-bis(4-chlorophenyl)-2,2,2-trichloroethane) is a persistent organic pollutant (POP) that has been identified by the World Health Organization as one of the POPs that require restrictions on production and use. Several methods have been proposed for mitigating residual POPs in soil and aquatic environments, including photocatalysis, bioremediation, thermal treatment, chemical degradation, soil washing, phytoremediation, and adsorption.[1−5] While photocatalytic degradation boasts promise as an eco-friendly technique for numerous organic contaminants, including DDT.[6,7] However, the efficiency of this approach is dependent on the concentration of DDT being sufficiently high. When dealing with low-concentration chemicals, the photocatalytic method exhibits reduced efficiency. Therefore, combining the photocatalytic process with an alternative strategy is regarded as a feasible approach. From this particular standpoint, adsorption is considered to be an appropriate supplementary technique for photocatalysis.[8] The combined use of adsorption and photocatalysis technology produces a synergistic effect, effectively utilizing the inherent advantages of each method. In adsorption−photocatalysis technology, the judicious selection of adsorbent materials proves crucial, for it dictates both the efficient capture of DDT molecules onto their surfaces and their subsequent degradation by the photocatalytically active sites.

MCM-41 (Mobil Composition of Matter No. 41) is a mesoporous material with a hierarchical structure from a family of silicate and aluminosilicate solids that were first developed by researchers at Mobil Oil Corporation.[9] MCM-41 has attracted considerable interest for possible applications in many fields as diverse as catalysis, drug delivery, adsorption, sensors, and optics due to its high surface area, low mass densities, and well-defined and adjustable pore structure.[10,11] It was reported that MCM-41 has a higher adsorption capacity for volatile organic compounds (VOCs) even at high vapor content than silicalite-1 and zeolite Y and commercial activated carbon.[12] MCM-41 derived from rice husk ash was employed for the effective elimination of polycyclic aromatic hydrocarbons, namely, naphthalene, benzo[*b*]-fluoranthene, benzo[*k*]fluoranthene, and benzo[*a*]pyrene,

Received: October 14, 2023
Revised: January 15, 2024
Accepted: January 22, 2024
Published: February 10, 2024

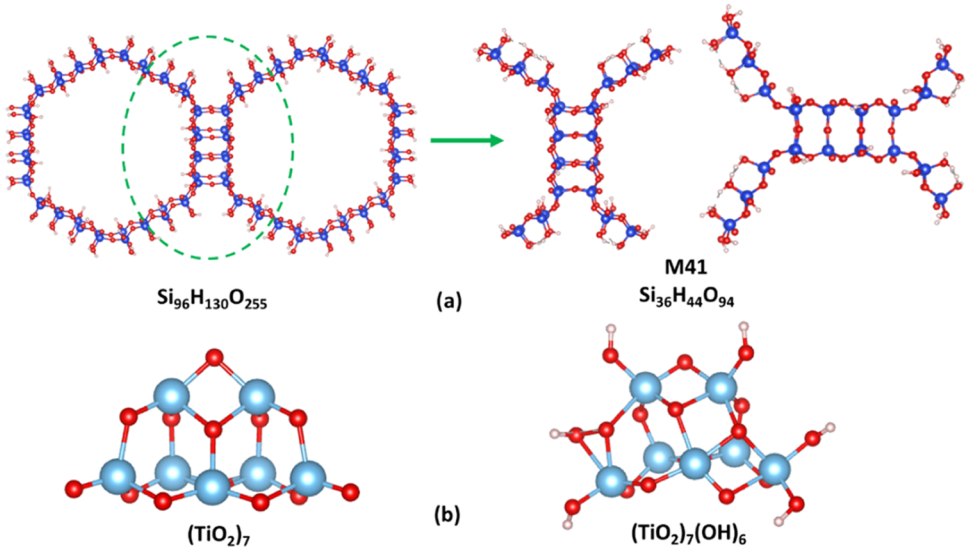

Figure 1. (a) Models of MCM-41 and M41; (b) models of $(TiO_2)_7$ and $(TiO_2)_7(OH)_6$. Color code: red: O, dark blue: Si, ivory: H, light blue: Ti.

from aqueous solutions. The removal efficiencies were remarkable, yielding percentages of 79.94, 94.34, 95.32, and 98.25%, respectively.[13] The incorporation of photocatalysts, such as titanium dioxide (TiO_2), onto MCM-41 has emerged as a promising technique for the degradation of various organic compounds. For example, a study found that TiO_2/MCM-41 composites with various titania contents were prepared by loading titania into the mesopores of MCM-41 molecular sieves by the sol−gel method and were used as photocatalysts to degrade Rhodamine B (RhB) and phenol.[14] The efficiency of organic contaminant removal was significantly increased compared with pure TiO_2. Reddy et al. successfully synthesized transition metal (Cr, V, Fe, Cu, Mn, Co, Ni, Mo, and La)-incorporated MCM-41 materials by a hydrothermal method.[15] The materials were loaded with TiO_2 via the sol−gel method and tested for the destruction of 4-chlorophenol in the presence of visible and UV light. The materials showed enhanced light absorption in the visible range and higher absorption in the UV range due to the presence of titania.

The interaction mechanisms between TiO_2 and MCM-41 are complex and vary depending on the method of incorporation. It was found that the one-pot synthesis of titanium into MCM-41 assists the incorporation and good dispersion of titanium ions into the mesochannel of MCM-41 frameworks. It also hinders the growth of large TiO_2 crystallites, which are beneficial to produce outstanding catalysts for the photocatalytic degradation of methylene blue and carbon monoxide oxidation.[16] Another work discovered that V-doped TiO_2 quantum dots (QDs) with numerous Ti^{3+} defects may be made by utilizing simple hydrolysis and MCM-41 as a support. Due to the quantum size effect and newly created defect- and dopant-mediated band levels, the QDs exhibit significant charge separation efficiency and photocatalytic activity.[17]

Despite extensive research on the applications of MCM-41, TiO_2, and the composite material TiO_2/MCM-41 in various contexts for treating organic compounds, there remains a notable gap in the existing literature concerning their application to DDT. Addressing this research gap, our study undertakes a pioneering effort to systematically investigate the potential of the bifunctional adsorption−photocatalysis material systems consisting of TiO_2 loaded on MCM-41 and MCM-41 modified with metal atoms (Al, Fe) for the adsorption and degradation of DDT.

2. MODELS AND COMPUTATIONAL METHODS

In order to construct the model of MCM-41, a specific structure denoted as M41, consisting of 174 atoms with the chemical formula $Si_{36}H_{44}O_9$, was extracted from an initial structure containing two double rings ($Si_{96}H_{130}O_{255}$) (Figure 1a). These double rings are representative of the mesoporous nature of MCM-41. As adsorption primarily occurs within the pores of MCM-41, the M41 structure is utilized to explore subsequent adsorption processes with a specific focus on molecules adsorbed within the concave regions. Subsequently, the initial M41 structure was modified by the incorporation of metal (Me) atoms, either aluminum (Al) or iron (Fe), resulting in a Si/Me atomic ratio of 35. The modified systems are referred to as M41(Al) and M41(Fe), respectively.

TiO_2 nanoparticles (TiO_2−NPs) in the shape of a $(TiO_2)_7$ cluster were chosen to be deposited on the surface of M41. In order to evaluate the performance of TiO_2−NPs in solutions, we further constructed and studied the structure of $(TiO_2)_7(OH)_6$ (Figure 1b), as previous findings demonstrating that the surface hydroxyl (OH) groups can alter both the geometric and electronic structure of TiO_2 clusters, resulting in alterations in optical properties.[18]

All structural and energy calculations were performed using density functional theory (DFT) within the context of the generalized gradient approximation (GGA) using the Perdew−Burke−Ernzerhof (PBE) exchange−correlation functional.[19] The double-ζ-polarized (DZP) basis set was utilized for the computations. The core electrons were treated by using norm-conserving pseudopotentials in the Kleinman−Bylander forms. An energy threshold of 250 Ryd was included. In order to incorporate van der Waals (vdW) interactions, we utilized the Grimme D2 approach, as described in the reference.[20] All calculations were performed using the open-source code SIESTA.[21]

The analysis of the adsorption process involves the examination of several key parameters, including intermolecular distance (d), adsorption energy (E_{ads}), Hirshfeld atomic charges (q) (to mitigate the impact of basis set dependency), and

https://doi.org/10.1021/acsomega.3c08050
ACS Omega 2024, 9, 7976−7985

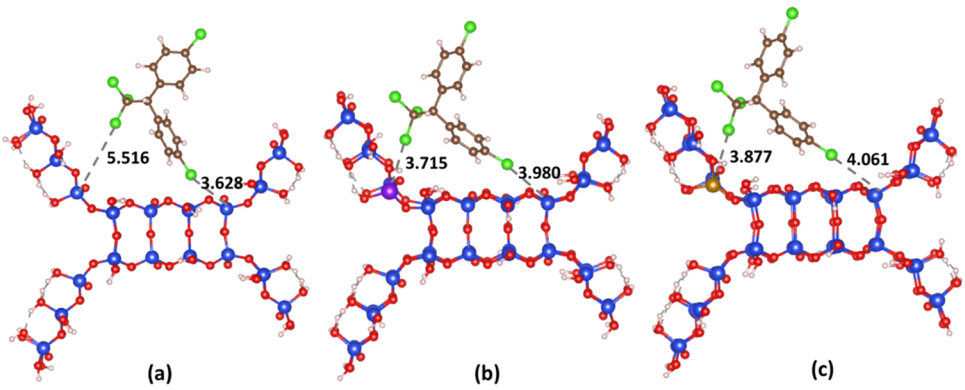

Figure 2. Optimized adsorption configurations: (a): DDT/M41, (b): DDT/M41(Al), and (c): DDT/M41(Fe); all key distances are in Å; color code: dark brown: C, green: Cl, violet: Al, light brown: Fe.

Table 1. Calculated Results for Adsorption of DDT on M41, M41(Al), and M41(Fe)

adsorption configuration	E_{ads}, kJ mol^{-1}	$\%E_{vdW}$	d, Å	q(DDT) e	BO
DDT/M41	−77.6(−48.1[a])	38%	5.516(Cl−Si)	−0.010	0.182
DDT/M41(Al)	−150.6 (−90.5[a])	40%	3.715(Cl−Al)	+0.049	0.154
DDT/M41(Fe)	−188.1 (−126.0[a])	33%	3.877(Cl−Fe)	−0.023	0.162

[a]Notes for Table 1: the values in parentheses represent the E_{ads}* value, excluding vdW interactions.

Wiberg bond orders (BO). Furthermore, molecular electrostatic potential, noncovalent interaction analysis, and bond path analysis were performed using Multiwfn software.[22,23]

The E_{ads} was calculated using two separate approaches, one incorporating vdW interactions and the other excluding them. This enabled us to assess the extent to which the vdW interactions contribute to the adsorption process. The calculation of E_{ads} and the determination of the percentage contribution of vdW interactions ($\%E_{vdW}$) were performed using the following formulas

$$E_{ads} = E_{adsorbate+absorbent} - E_{adsorbate} - E_{adsorbent} \quad (1.a)$$

$$\%E_{vdW} = \frac{E_{ads} - E_{ads}^{*}}{E_{ads}} \quad (1.b)$$

where E_{ads} and E_{ads}* are the adsorption energy with and without accounting for vdW interactions. To isolate the contribution of van der Waals interactions to each adsorption process, two separate optimization calculations were performed: one using DFT-D2 (to get E_{ads}*) and one using only DFT (to get E_{ads}).

The electron absorption spectra were calculated by employing real-time time-dependent density functional theory (RT-TDDFT) with the *x*TB2 Hamiltonian. The band gap (E_{gap}) was computed as the energy difference between the highest occupied molecular orbital (HOMO) and the lowest unoccupied molecular orbital (LUMO) of the systems. The optical spectrum calculations were performed using DFTB+ software.[24]

3. RESULTS AND DISCUSSIONS

3.1. Adsorption of DDT on M41, M41(Al), and M41(Fe).

Figure 2 illustrates the optimized adsorption structures of DDT on M41, M41(Al), and M41(Fe). Table 1 presents the calculated results for the DDT adsorption processes on the M41 systems.

The obtained computed results demonstrate that the adsorption of DDT on M41 and modified M41 materials is energetically favorable, as evidenced by the negative values of the adsorption energy. The replacement of a Si atom with either an Al or Fe atom results in a decrease in the E_{ads} values, suggesting that the adsorption process becomes more favorable from a thermodynamic perspective. The charge transfer between DDT and the M41 systems is negligible, fluctuating within the range of 0.01−0.05 e, along with the formation of very weak covalent bonds, with values ranging from 0.154 to 0.182. Notably, the changes in BO values do not follow a pattern similar to E_{ads}. However, it is important to highlight that these BO values only account for the formation of covalent bonds, if present. Weak interactions and noncovalent bonds are not considered in the BO values. Therefore, it is important to acknowledge that the utilization of the BO for evaluating the adsorption capacity of adsorbents toward DDT is a relative indicator.

In order to clarify the impact of Si substitution with Al and Fe, we conducted an analysis of the molecular electrostatic potential (MEP) at a specific point (r) near a molecule. This characteristic represents the interaction energy between the charge distribution of the molecule and a positively charged test particle (a proton) located at r, considering the electrical charge cloud generated by the molecule's electrons and nuclei. While the external test charge does not induce any changes in the molecular charge distribution, resulting in no polarization, the electrostatic potential of a molecule remains a useful tool for evaluating the molecule's reactivity toward reactants with positive or negative charges.[25]

Within the linear combination of atomic orbitals approximation, MEP at $\boldsymbol{r}$ point in the vicinity of a molecule is defined as follows:

$$V(\boldsymbol{r}) = \sum_{A} \frac{Z_A}{|\boldsymbol{r} - \boldsymbol{R}_A|} - \sum_{\mu} \sum_{\nu} \boldsymbol{P}_{\mu\nu} \int \frac{\varphi_\mu(\boldsymbol{r}')\varphi_\nu(\boldsymbol{r}')}{|\boldsymbol{r} - \boldsymbol{r}'|} d\boldsymbol{r}' \quad (2)$$

where Z_A is the charge of core A, $\boldsymbol{R}_A$ is the position vector of atom A, $\boldsymbol{P}_{\mu\nu}$ is the first-order density matrix $\boldsymbol{P}$, and φ is a real atomic basis function.

https://doi.org/10.1021/acsomega.3c08050
ACS Omega 2024, 9, 7976−7985

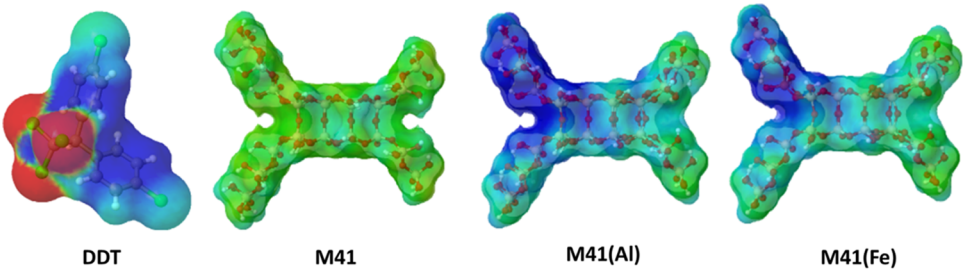

Figure 3. Calculated molecular electrostatic potentials of DDT, M41, M41(Al), and M41(Fe) vary between −0.5 (in red) and +0.5 (in navy blue).

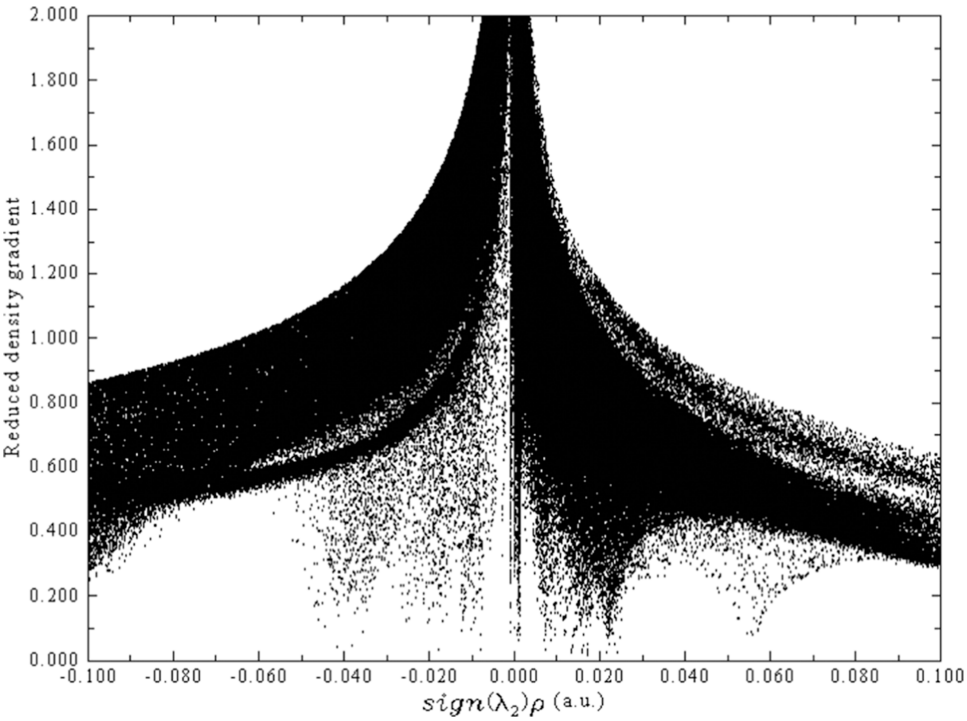

Figure 4. 2D map of the sign$(\lambda_2)\rho(\boldsymbol{r})$ function for the DDT/M41 system.

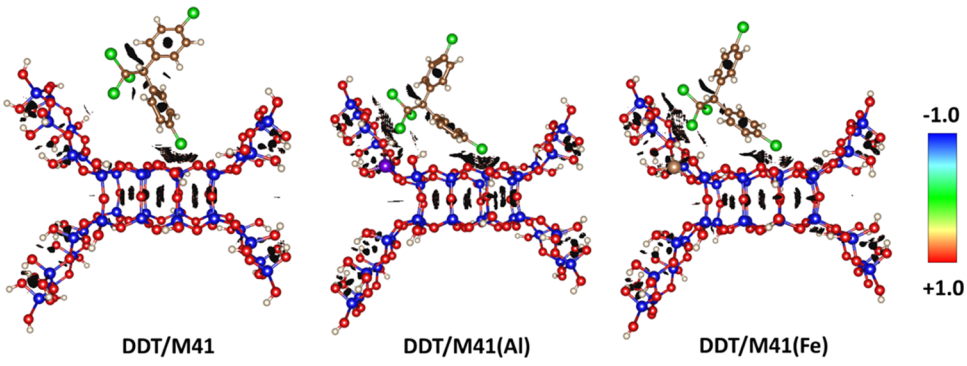

Figure 5. Image depicting $sign(\lambda_2)\rho(\boldsymbol{r})$ at an isovalue of 0.30 au for the adsorption of DDT on M41, M41(Al), and M41(Fe).

The calculated MEPs for the studied systems are listed in Figure 3.

The results indicate that the substitution of Si with Al or Fe leads to alterations in V(r) of the surrounding environment. Specifically, the $V(\boldsymbol{r})$ value becomes more positive within the substitution region, which signifies an enhanced electrostatic interaction with negatively charged atoms or groups such as Cl atoms in DDT. Considering that MEP solely represents the electrostatic component of interactions, alternative methodologies are required to investigate interactions that entail electron participation. Therefore, the noncovalent interaction (NCI) analysis was performed. This approach, based on Bader's AIM theory, as described in the previous publication,[26] makes use of the reduced density gradient (RDG) function. When the RDG function registers within the range of 0 to a medium value, it signifies a region of weak interaction

https://doi.org/10.1021/acsomega.3c08050
ACS Omega 2024, 9, 7976−7985

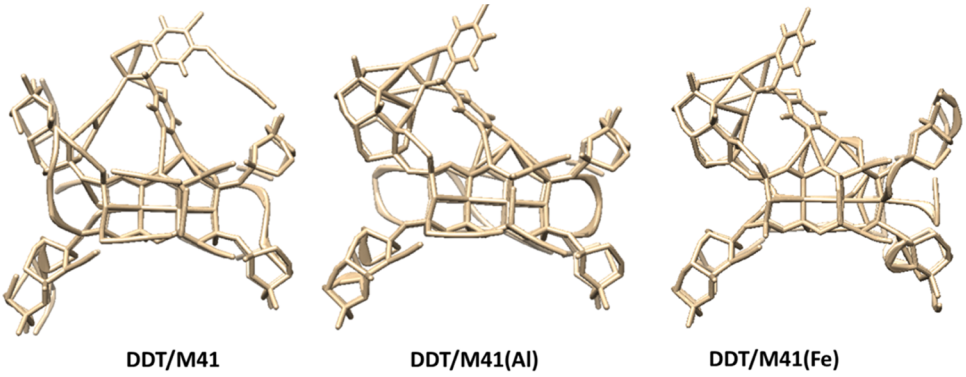

Figure 6. Bond paths of the DDT systems on M41, DDT/M41(Al), and M41(Fe).

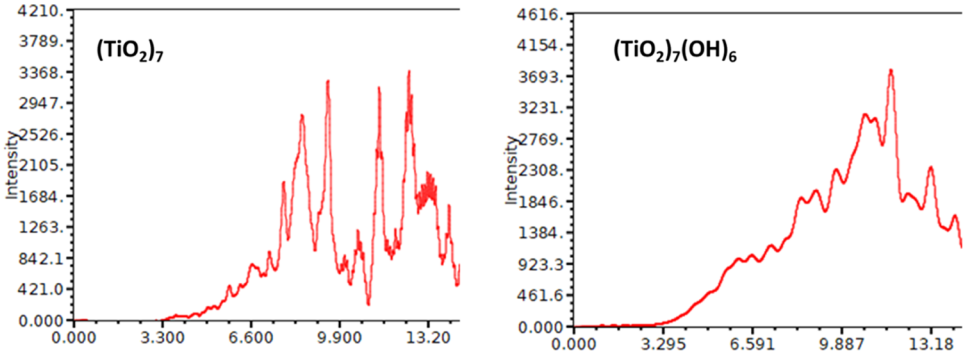

Figure 7. Calculated spectra for $(TiO_2)_7$ and $(TiO_2)_7(OH)_6$.

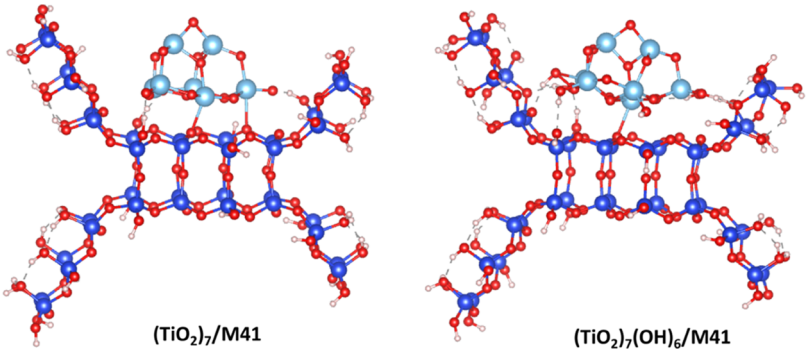

Figure 8. Optimized structures of the $(TiO_2)_7$/M41 and $(TiO_2)_7(OH)_6$/M41 systems.

$$\mathrm{RDG}(\boldsymbol{r}) = \frac{1}{2(3\pi^2)^{1/3}} \frac{|\nabla\rho(\boldsymbol{r})|}{\rho(\boldsymbol{r})^{4/3}} \tag{3}$$

where ρ denotes the electron density.

The dependency of RDG on the real space function $\mathrm{sign}(\lambda_2)\rho$ is depicted in Figure 4. It is clear that the DDT/M41 system exhibits all three types of weak interactions. The hydrogen bond and halogen bond are evident in the negative region of the function. Meanwhile, the vdW interaction and steric effects are noticeable in the positive region of this function.

The results depicted in Figure 5 demonstrate the presence of pronounced dark regions leaning toward the negative side, indicating bonds of the hydrogen and/or halogen bond types. The strength of these bonds increases in the M41(Al) and M41(Fe) systems, resulting in a more negative adsorption energy. Notably, the results have revealed the formation of halogen bonds between DDT and various types of M41. In order to further investigate the assessment of weak interactions formed between DDT and the adsorbents, an analysis was conducted on critical points (CPs) and bond pathways. Critical points (CPs) are locations in a system where the electron density reaches a maximum or minimum value. For example, in covalent bonds formed by sigma bonds, the region of maximum electron density (at least locally) corresponds to the bond path, which connects the nuclei.

The results of the bond paths in Figure 6 clearly illustrate the formation of (weak) bonds between DDT and the M41 systems, facilitated through halogen bonds and C−H···O interactions. Significantly, the quantity of bonds increases when the transition is from unmodified M41 to those modified with Al and Fe.

3.2. Properties of TiO_2−NPs and TiO_2 Dispersed on M41. The number of surface hydroxyl (−OH) groups on TiO_2 is well known to be dependent on the method used to synthesize TiO_2 NPs.[27] In this study, we will examine two contrasting scenarios: (i) TiO_2 with the lack of surface −OH groups in the

https://doi.org/10.1021/acsomega.3c08050
ACS Omega 2024, 9, 7976−7985

Table 2. Calculated Results for $(TiO_2)_7$ and $(TiO_2)_7(OH)_6$ Dispersed on M41

systems	E_{int}, kJ mol^{-1}	$q(TiO_2)$, e	BO	E_{gap}, eV
$(TiO_2)_7$/M41	−494.2	−0.253	Ti−O(M41) = 0.951	3.17
$(TiO_2)_7(OH)_6$/M41	−558.0	−0.422	Ti−O(M41) = 0.361	3.14

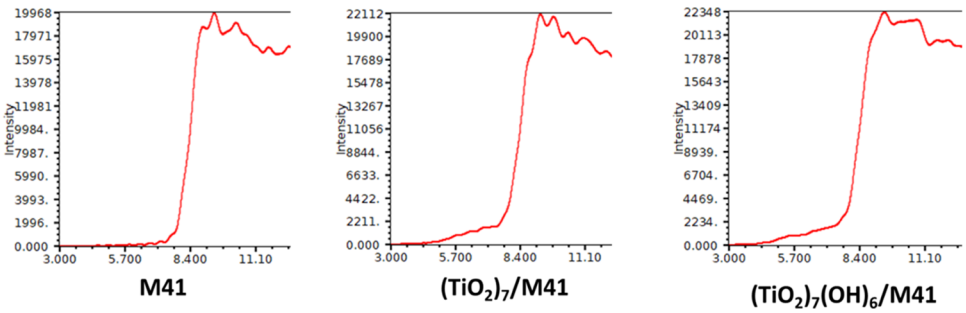

Figure 9. Calculated spectra of M41, $(TiO_2)_7$/M41, and $(TiO_2)_7(OH)_6$/M41.

form of $(TiO_2)_7$ and (ii) TiO_2 with the existence of surface −OH groups in the form of $(TiO_2)_7(OH)_6$.

(i) In the absence of −OH groups, unsaturated Ti atoms can potentially form bonds with oxygen atoms from M41. If this bond is overly robust and the TiO_2NPs are small, it may lead to a significant modification in the electronic structure and optical characteristics of TiO_2.

(ii) When there are −OH groups saturating certain Ti atoms, it might prevent the formation of Ti−O bonds (with M41). In such cases, the interaction between TiO_2 and M41 is anticipated to be rather moderate, leading to negligible modifications in the optical characteristics of $TiO_2(OH)_n$.

3.2.1. Optical Properties of $(TiO_2)_7$ and $(TiO_2)_7(OH)_6$. The results of the electronic absorption spectra computed using the RT-TDDFT method for the systems are depicted in Figure 7.

The calculated E_{gap} for $(TiO_2)_7$ and $(TiO_2)_7(OH)_6$ are 4.19 and 3.67 eV, respectively. The computed E_{gap} value for the $(TiO_2)_7$ system is in good agreement with previous investigations.[28] The incorporation of hydroxyl groups into a $(TiO_2)_7$ structure decreases the E_{gap} of the clusters, resulting in an enhanced ability to absorb photons.

3.2.2. Deposition of $(TiO_2)_7$ and $(TiO_2)_7(OH)_6$ onto the M41 Support Material. Optimized structures of $(TiO_2)_7$/M41 and $(TiO_2)_7(OH)_6$/M41 are presented in Figure 8.

The presence of −OH groups on TiO_2 significantly inhibits the occurrence of chemically bound Ti···O(M41) interactions. The optimized structure of $TiO_2(OH)$/M41 demonstrates that Ti atoms that are fully occupied by −OH groups do not establish chemical bonds with the −OH atoms in the M41 structure.

The findings presented in Table 2 reveal that both $(TiO_2)_7$ and $(TiO_2)_7(OH)_6$ exhibit significant interactions with M41, as indicated by the notably negative interaction energies (E_{int}), and the significantly negative energy value (−494.2 and −558.0 kJ mol^{-1}) suggests a strong chemisorption mechanism between $(TiO2)_7$ and $(TiO_2)_7(OH)_6$ with MCM-41, implying the formation of covalent bonds. Covalent bonds play a minor role in the interaction between $(TiO_2)_7(OH)_6$ and M41, as shown by the relatively low bond order values between the atoms in TiO_2 and those in M41. However, there is a notable transfer of the charge from M41 to TiO_2. This can be explained by the primary mode of interaction observed in the $(TiO_2)_7(OH)_6$/M41 system, which is attributed to hydrogen bonding. In contrast, the interaction between $(TiO_2)_7$ and M41 involves the formation of weak Ti···O(M41) bonds. The total covalent bond order formed between TiO_2 and M41 is significantly higher compared to the case of $(TiO_2)_7(OH)_6$/M41. Charge is transferred from M41 to TiO_2 via the formation of interactions such as $Ti^{5+}\cdots O^{2-}$(M41) and $Ti-O-H^{+1}\cdots O^{2-}$(M41). This additional electron receiving may be responsible for the decrease in E_{gap} when compared to isolated TiO_2, as it alters the electronic structure of TiO_2. The magnitude of the E_{gap} for M41 is significantly high (10.48 eV), implying that it does not possess semiconductor properties. The E_{gap} values of $(TiO_2)_7$/M41 and $(TiO_2)_7(OH)_6$/M41 exhibit a notable degree of similarity, with both values being much reduced compared with when these entities are not affixed onto the M41 support material.

The UV−vis spectra in Figure 9 for the $(TiO_2)_7$/M41 and $(TiO_2)_7(OH)_6$/M41 systems do not differ significantly. However, they differ from the M41 spectrum in the range from 3.0 to below 8.4 eV, as this corresponds to the optical absorption region of TiO_2.

The HOMO and LUMO images of $(TiO_2)_7$/M41 and $(TiO_2)_7(OH)_6$/M41 (Figure 1 and the Supporting Information) clearly illustrate two main points. (i) The combined system's HOMO and LUMO are predominantly located in the TiO_2 region, thus preserving the optical properties of TiO_2. (ii) Due to the weaker chemical interaction of $(TiO_2)_7(OH)_6$ compared to $(TiO_2)_7$ with M41, the HOMO of the $(TiO_2)_7(OH)_6$/M41 system is mostly concentrated in the TiO_2 region. In other words, the corresponding electron density is higher, potentially leading to a better photocatalytic efficiency. The HOMO and LUMO in the TiO_2 component of the $(TiO_2)_7$/M41 and $(TiO_2)_7(OH)_6$/M41 systems suggests the existence of a synergistic catalytic enhancement effect between M41 and the TiO_2 catalyst.

Hence, the analysis and calculations indicate that using M41 as a carrier for TiO_2 can enhance catalytic efficiency by (i) reducing the E_{gap} of TiO_2, (ii) maintaining the photocatalytic activity of TiO_2, and (iii) facilitating the favorable dispersion of TiO_2 NPs on M41, owing to their notably negative interaction energy. When titanium dioxide $(TiO_2)_7$ possesses surface hydroxyl (−OH) groups, it may restrict undesirable chemical interactions with M41, hence enhancing its catalytic efficiency.

https://doi.org/10.1021/acsomega.3c08050
ACS Omega 2024, 9, 7976−7985

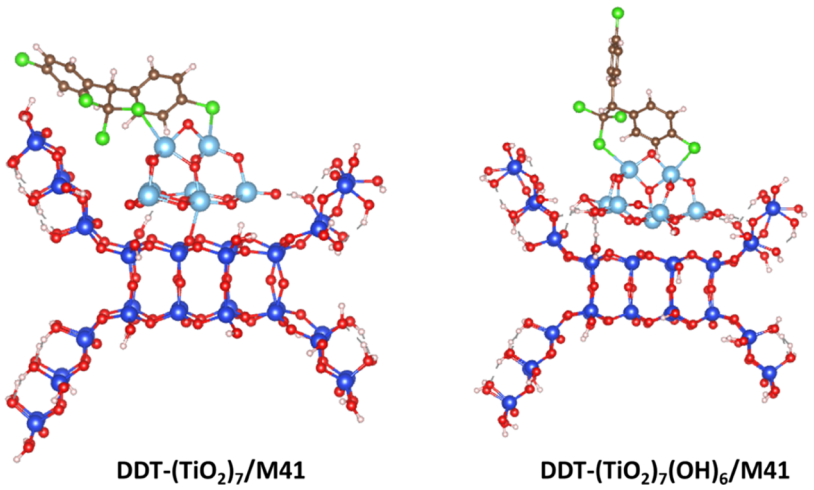

Figure 10. Optimized adsorption configuration of DDT on $(TiO_2)_7$/M41 and $(TiO_2)_7(OH)_6$/M41.

Table 3. Calculated Results for Adsorption of DDT on $(TiO_2)_7$/M41 and $(TiO_2)_7(OH)_6$/M41

systems	E_{int}, kJ mol^{-1}	q(DDT), e	BO	E_{gap}, eV
DDT-$(TiO_2)_7$/M41	−461.3	+0.670	Cl−Ti = 0.858	3.22
DDT-$(TiO_2)_7(OH)_6$/M41	−200.6	+0.486	Cl−Ti = 0.810	3.37

4. ADSORPTION AND DEGRADATION OF DDT ON TIO_2/M41 SYSTEMS

4.1. Adsorption of DDT on TiO_2/M41. The research findings on the adsorption of DDT onto the $(TiO_2)_7$/M41 and $(TiO_2)_7(OH)_6$/M41 systems demonstrate a strong interaction between DDT and the catalyst, facilitated by the formation of Cl···Ti bonds (Figure 10 and Table 3).

The findings presented in Table 3 reveal that the overall charge of DDT molecule is positive compared to its isolated state. This indicates an electron transfer toward TiO_2 upon adsorption of DDT on this system. The substantial positive charge signifies an effective adsorption process, which differs from the adsorption of DDT on M41 (Table 1). The obtained adsorption energy demonstrates that DDT is strongly adsorbed on the $(TiO_2)_7$/M41 system, as evidenced by the notably negative E_{int} energy; the very negative adsorption energy (−461.3 kJ mol^{-1}) when DDT is adsorbed on the $(TiO_2)_7$/M41 system leads to the prediction that chemical adsorption has occurred. On the other hand, DDT exhibits moderate adsorption on the $(TiO_2)_7(OH)_6$/M41 system, with an adsorption energy found to be less than 50% compared to the $(TiO_2)_7$/M41 system; however, the bond order formed between Cl and Ti is still very high (0.810). Consequently, when TiO_2 NPs are dispersed on M41, the resulting system exhibits an enhanced capability to adsorb DDT due to the formation of chemical bonds. This is in contrast to situations in which M41 does not contain TiO_2 nanoparticles.

4.2. Degradation of DDT on TiO_2/M41. The typical mechanism utilized to describe the degradation of various compounds in photocatalysis investigations relies on the generation of electron−hole pairs by the absorption of light. For example, the photocatalytic mechanism using a TiO_2/g-C_3N_4 catalyst is often explained as follows:

(i) Within the conduction band—CB (HOMOs) of TiO_2, a reaction occurs involving the formation of a superoxide anion ($O_2^{\bullet-}$) by the addition of a photogenerated electron (e^-), as represented by the equation $O_2 + e^- \rightarrow O_2^{\bullet-}$

(ii) Within the valence band—VB (LUMOs) of g-C_3N_4, a chemical reaction occurs involving the generation of hydroxyl radicals ($OH^{\bullet}$) through the production of free hydroxyl radical OH− and a positively charged hole (h^+): $OH^- + h^+ \rightarrow OH^{\bullet}$

The $O_2^{\bullet-}$and $OH^{\bullet}$ radicals have high oxidizing properties, allowing them to be capable of oxidizing and decomposing various compounds, including DDT.[29] The presence of dissolved oxygen in water is necessary for the proposed mechanism. We provisionally refer to this mechanism as the indirect DDT degradation mechanism. In this study, we propose an additional degradation mechanism, the direct DDT degradation mechanism, which does not require the presence of dissolved organic acid or dissolved O_2.

First, we evaluated the photogenerated electron acceptance abilities of two agents, O_2 and DDT, by calculating the vertical energy values associated with the electron acceptance processes using the B3LYP/def2-SVP method in a water solvent according to the conductor-like polarizable continuum model as follows:

$$O_2 + e^- \rightarrow O_2^{\bullet-},\ \Delta_r E(\text{vertical}) = -2.07\ \text{eV}$$

$$DDT + e^- \rightarrow DDT^{\bullet-},\ \Delta_r E(\text{vertical}) = -1.23\ \text{eV}$$

The rationale for studying these processes in a "vertical" manner stems from the Franck−Condon principle, indicating that photon absorption occurs much faster than nuclear motion. The results indicate that in the presence of O_2 in water, O_2 will predominantly accept electrons from the VB of TiO_2 first. Otherwise, DDT will accept the electron (when considering a solution with only two electron acceptors, O_2 and DDT). The electron acceptance process of DDT is energetically favorable. Moreover, if the electron originates from the VB of TiO_2, it possesses high energy (as it has absorbed energy from photons, at least equal to E_{gap}).

Following electron acceptance, $DDT^{\bullet-}$ is highly unstable and promptly undergoes the subsequent transformation process.

https://doi.org/10.1021/acsomega.3c08050
ACS Omega 2024, 9, 7976−7985

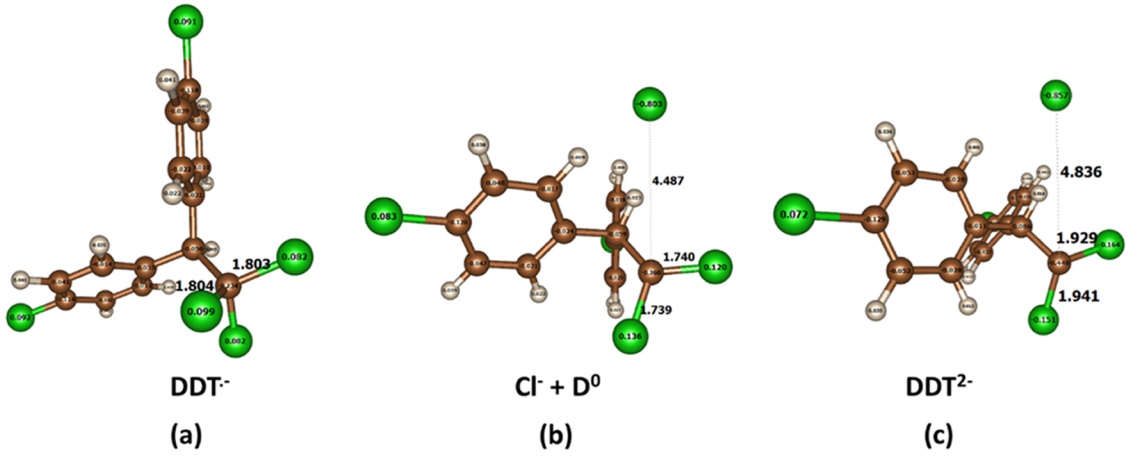

Figure 11. Atomic charge and C···Cl distances of (a) $DDT^{\bullet-}$, (b) $Cl^- + D^0$, and (c) DDT^{2-}.

$$DDT^{\bullet-} \rightarrow Cl^- + D^0,\ \Delta_r E = -199.4\ \text{kJ mol}^{-1}$$

where D^0 represents the remaining (energy-minimized) structure after extracting Cl^- from DDT. The optimized structures of $DDT^{\bullet-}$, $Cl^- + D^0$, and DDT^{2-} are shown in Figure 11.

The assumption that the transformation process of $DDT^{\bullet-}$ takes place spontaneously is based on:

(i) An analysis of the contributions of atomic orbitals (AOs) to the LUMO of DDT and HOMO (SOMO) of $DDT^{\bullet-}$

Concerning the LUMO of DDT: this corresponds to the electron-accepting MO of DDT. The coefficients of the wave function for this MO are employed to calculate the percentage contribution of each atom to the LUMO of DDT. There are 14 C atoms, with the least contributing atom at 0.4% and the highest at 14% (atom C1); 9 H atoms, with the highest contributing atom at 0.3%; 5 Cl atoms, with the least contributing atom at 1%, and the highest at 8% (atom Cl27).

In regards to the HOMO of $DDT^{\bullet-}$: this aligns with the LUMO of DDT that has accepted an electron. The coefficients of the wave function for this MO are used to calculate the percentage contribution of each atom to the HOMO of $DDT^{\bullet-}$. There are 14 C atoms, with the least contributing atom at 1% and the highest at 13% (atom C1); all 9 H atoms do not contribute to the LUMO; 5 Cl atoms, with the least contributing atom at 1% and the highest at 7%.

Thus, when DDT accepts an electron into the antibonding MO (LUMO), it leads to a reduction in bond order on the atoms, most notably C1 and Cl. However, due to C having a valence of 4, while Cl has a valence of 1, the breaking of the C−Cl bond is clearly observed.

(ii) The process of optimizing the structure of $DDT^{\bullet-}$ consistently yields Cl^- and D^0, indicating that this process does not pass through a transition state.

The calculations revealed that DDT can acquire electrons when it interacts with reducing agents. This is particularly evident when an additional electron is introduced, resulting in the cleavage of a C−Cl bond and the formation of Cl^-. It is noteworthy that the calculations also demonstrate that when DDT accepts two electrons, not only does it lead to the breaking of a C−Cl bond, but the remaining two C−Cl bonds in the original $-CCl_3$ group also undergo elongation, thus facilitating subsequent cleavage (refer to Figure 11c). Consequently, one effective method for degrading DDT in water is to allow it to accept additional electrons.

Regarding DDT chemically bonded to TiO_2, this interaction may bring about alterations in the optical properties of TiO_2. This effect is particularly pronounced when the size (i.e., the number of atoms) of TiO_2 is smaller than that of DDT, as observed in a system with 21 atoms $(TiO_2)_7$. Figure 2 (Supporting Information) provides a visual representation of the HOMO and LUMO states of DDT bonded to TiO_2/M41. While the HOMO is predominantly situated on TiO_2, the LUMO is mainly concentrated on DDT. This sets the stage for a direct photocatalytic process: an electron residing in the HOMO of TiO_2 absorbs a photon with adequate energy, promptly transferring into DDT bonded to TiO_2 due to the preceding adsorption process. This sequence leads to the cleavage of the C−Cl bond, ultimately resulting in the degradation of DDT.

5. CONCLUSIONS

Through a theoretical investigation, the study of the structure and properties of $(TiO2)_7$ and M41 revealed several important findings regarding their adsorption and photocatalytic degradation capabilities for DDT.

First, it has been demonstrated that DDT is physically adsorbed on M41. The introduction of Al and Fe impurities through the substitution of Si in the M41 framework enhances the adsorption capacity. This adsorption process is primarily driven by van der Waals interactions, halogen bonds, and hydrogen bonds.

Second, TiO_2 NPs interact effectively with M41. M41 serves a dual function, acting as both a catalytic support material and exhibiting a synergistic effect by reducing the energy gap of TiO_2. The presence of surface −OH groups on TiO_2 NPs leads to better efficiency: (i) DDT is not excessively adsorbed onto $(TiO_2)_7(OH)_6$, facilitating the desorption process of products; (ii) $(TiO_2)_7(OH)_6$ does not undergo overly strong chemical interactions with M41, limiting its impact on the photocatalytic activity of TiO_2.

Third, a novel direct mechanism for DDT degradation has been proposed for the first time. This mechanism involves the direct acceptance of electrons from the TiO_2 photocatalyst, resulting in DDT degradation through the cleavage of the C−Cl bond. In systems with small-sized TiO_2 NPs, a process of DDT

https://doi.org/10.1021/acsomega.3c08050
ACS Omega 2024, 9, 7976−7985

adsorption may precede degradation through a photochemical mechanism that involves the direct transfer of electrons from the highest occupied molecular orbital (HOMO) of TiO_2 to the lowest unoccupied molecular orbital (LUMO) of DDT. This novel process demonstrates significant promise for treating low-concentration DDT in water due to the key role played by the initial adsorption process on TiO_2. Furthermore, its direct nature has the potential to explain other instances of photochemical oxidation by different photocatalysts in the absence of oxygen in water. While further experimentation is necessary to fully validate this mechanism, its potential applications extend beyond DDT to other environmental contaminants, contributing to a deeper understanding of photocatalysis under oxygen-free conditions.

■ ASSOCIATED CONTENT

Supporting Information

The Supporting Information is available free of charge at https://pubs.acs.org/doi/10.1021/acsomega.3c08050.

HOMO and LUMO of $(TiO_2)_7$/M41 and $(TiO_2)_7(OH)_6$/M41, HOMO and LUMO of DDT-$(TiO_2)_7$/M41 and DDT-$(TiO_2)_7(OH)_6$/M41 (PDF)

■ AUTHOR INFORMATION

Corresponding Author

Nguyen Ngoc Ha − *Hanoi National University of Education, Hanoi 100000, Vietnam*; Email: hann@hnue.edu.vn

Authors

Nguyen Thi Thu Ha − *Hanoi National University of Education, Hanoi 100000, Vietnam*; orcid.org/0000-0002-9979-2399

Hoang Lan Ngo − *Hanoi National University of Education, Hanoi 100000, Vietnam*

Thi Be Pham − *Tay Nguyen University, Buon Me Thuat 630000 Daklak, Vietnam*

Nguyen Hoang Hao − *College of Education, Vinh University, Vinh 460000, Vietnam*

Cong Trinh Bui − *Institute for Technology of Radioactive and Rare Elements, Hanoi 100000, Vietnam*

Thi Lan Phung − *Hanoi National University of Education, Hanoi 100000, Vietnam*

Le Minh Cam − *Hanoi National University of Education, Hanoi 100000, Vietnam; Thanh Do University, Hanoi 13200, Vietnam*

Complete contact information is available at: https://pubs.acs.org/10.1021/acsomega.3c08050

Notes

The authors declare no competing financial interest.

■ ACKNOWLEDGMENTS

This work is funded by the Ministry of Science and Technology under grant no. ĐTĐL.CN-66/19.

■ REFERENCES

(1) Sun, B.; Li, Q.; Zheng, M.; Su, G.; Lin, S.; Wu, M.; Li, C.; Wang, Q.; Tao, Y.; Dai, L.; Qin, Y.; Meng, B. Recent advances in the removal of persistent organic pollutants (POPs) using multifunctional materials: a review. *Environ. Pollut.* **2020**, *265* (Pt A), No. 114908, DOI: 10.1016/j.envpol.2020.114908.

(2) Purnomo, A.; Mori, T.; Kamei, I.; Kondo, R. Basic studies and applications on bioremediation of DDT: A review. *Int. Biodeterior. Biodegrad.* **2011**, *65* (7), 921−930.

(3) Pariatamby, A.; Kee, Y. Persistent organic pollutants management and remediation. *Procedia Environ. Sci.* **2016**, *31*, 842−848.

(4) Taha, M. R.; Mobasser, S. Adsorption of DDT and PCB by Nanomaterials from Residual Soil. *PLoS One* **2015**, *10* (12), No. e0144071.

(5) Hale, S. E.; Tomaszewski, J. E.; Luthy, R. G.; Werner, D. Sorption of dichlorodiphenyltrichloroethane (DDT) and its metabolites by activated carbon in clean water and sediment slurries. *Water Res.* **2009**, *43* (17), 4336−4346.

(6) Borello, R.; Minero, C.; Pramauro, E.; Pelizzetti, E.; Serpone, N.; Hidaka, H. Photocatalytic degradation of DDT mediated in aqueous semiconductor slurries by simulated sunlight. *Environ. Toxicol. Chem.* **1989**, *8* (11), 997−1002.

(7) Ananpattarachai, J.; Kajitvichyanukul, P. Photocatalytic degradation of p,p′-DDT under UV and visible light using interstitial N-doped TiO_2. *J. Environ. Sci. Health., Part B* **2015**, *50* (4), 247−260.

(8) Ha, N. T. T.; Be, P. T.; Ha, N. N. Adsorption of lindane (g-hexachlorocyclohexane) on nickel modified graphitic carbon nitride: a theoretical study. *RSC. Adv.* **2021**, *11* (34), 21048−21056, DOI: 10.1039/D1RA03797H.

(9) Kresge, C. T.; Leonowicz, M. E.; Roth, W. J.; Vartuli, J. C.; Beck, J. S. Ordered mesoporous molecular sieves synthesized by a liquid-crystal template mechanism. *Nature* **1992**, *359* (6397), 710−712.

(10) Kruk, M.; Jaroniec, M.; Sayari, A. Adsorption Study of Surface and Structural Properties of MCM-41 Materials of Different Pore Sizes. *J. Phys. Chem. B* **1997**, *101* (4), 583−589.

(11) Khan, D.; Shaily. Synthesis and catalytic application of organo-functionalized MCM-41 catalyst are reviewed. *Appl. Organomet. Chem.* **2023**, *37* (3), No. e7007, DOI: 10.1002/aoc.7007.

(12) Zhao, X. S.; Ma, Q.; Lu, G. Q. VOC removal: Comparison of MCM-41 with hydrophobic zeolites and activated carbon. *Energy Fuels* **1998**, *12* (6), 1051−1054.

(13) Costa, J. A. S.; Sarmento, V. H. V.; Romão, L. P. C.; Paranhos, C. M. Adsorption of organic compounds on mesoporous material from rice husk ash (RHA). *Biomass Convers. Biorefin.* **2020**, *10* (4), 1105−1120, DOI: 10.1007/s13399-019-00476-4.

(14) Tian, L.; Liu, H.; Gao, Y. Degradation and adsorption of rhodamine B and phenol on TiO2/MCM-41. *Kinet. Catal.* **2012**, *53* (5), 554−559, DOI: 10.1134/S0023158412050175.

(15) Reddy, E. P.; Davydov, L.; Smirniotis, P. G. Characterization of Titania Loaded V-, Fe-, and Cr-Incorporated MCM-41 by XRD, TPR, UV−vis, Raman, and XPS Techniques. *J. Phys. Chem. B* **2002**, *106* (13), 3394−3401.

(16) Hassan, H. M. A.; Mohamed, S. K.; Ibrahim, A. A.; AwaBetiha, M. A.; El-Sharkawy, E. A.; Mousa, A. A. A comparative study of the incorporation of TiO_2 into MCM-41 nanostructure via different approaches and its effect on the photocatalytic degradation of methylene blue and CO oxidation. *React. Kinet,, Mech. Catal.* **2017**, *120* (2), 791−807, DOI: 10.1007/s11144-016-1124-4.

(17) Pan, L.; Wang, S.; Zou, J. J.; Huang, Z. F.; Wang, L.; Zhang, X. Ti^{3+}-defected and V-doped TiO_2 quantum dots loaded on MCM-4. *Chem. Commun.* **2014**, *50* (8), 988−990.

(18) Miroshnichenko, O.; Auvinen, S.; Alatalo, M. A DFT study of the effect of OH groups on the optical, electronic, and structural properties of TiO2 nanoparticles. *Phys. Chem. Chem. Phys.* **2015**, *17* (7), 5321−5327.

(19) Perdew, J. P.; Burke, K.; Ernzerhof, M. Generalized Gradient Approximation Made Simple. *Phys. Rev. Lett.* **1996**, *77* (18), 3865−3868.

(20) Grimme, S. Density functional theory with London dispersion corrections. *WIREs Comput. Mol. Sci.* **2011**, *1* (2), 211−228.

(21) José, M. S.; Emilio, A.; Julian, D. G.; Alberto, G.; Javier, J.; Pablo, O.; Daniel, S. P. The SIESTA method for ab initio order-N materials Simulation. *J. Phys.: Condens. Matter* **2002**, *14* (11), 2745−2749, DOI: 10.1088/0953-8984/14/11/302.

(22) Lu, T.; Chen, F. Multiwfn: A multifunctional wavefunction analyzer. *J. Comput. Chem.* **2012**, *33* (5), 580−592.
(23) Zhang, J.; Lu, T. Efficient evaluation of electrostatic potential with computerized optimized code. *Phys. Chem. Chem. Phys.* **2021**, *23* (36), 20323−20328.
(24) Hourahine, B.; Aradi, B.; Blum, V.; Bonafé, F.; Buccheri, A.; Camacho, C.; Cevallos, C.; Deshaye, M. Y.; Dumitrică, T.; Dominguez, A.; Ehlert, S.; Elstner, M.; van der Heide, T.; Hermann, J.; Irle, S.; Kranz, J. J.; Köhler, C.; Kowalczyk, T.; Kubař, T.; Lee, I. S.; Lutsker, V.; Maurer, R. J.; Min, S. K.; Mitchell, I.; Negre, C.; Niehaus, T. A.; Niklasson, A. M. N.; Page, A. J.; Pecchia, A.; Penazzi, G.; Persson, M. P.; Řezáč, J.; Sánchez, C. G.; Sternberg, M.; Stöhr, M.; Stuckenberg, F.; Tkatchenko, A.; Yu, V. W. z.; Frauenheim, T. DFTB$^+$, a software package for efficient approximate density functional theory based atomistic simulations. *J. Chem. Phys.* **2020**, *152* (12), No. 124101, DOI: 10.1063/1.5143190.
(25) Johnson, E. R.; Keinan, S.; Mori-Sánchez, P.; Contreras-García, J.; Cohen, A. J.; Yang, W. Revealing Noncovalent Interactions. *J. Am. Chem. Soc.* **2010**, *132* (18), 6498−6506.
(26) Wu, C. Y.; Tu, K. J.; Deng, J. P.; Lo, Y. S.; Wu, C. H. Markedly Enhanced Surface Hydroxyl Groups of TiO_2 Nanoparticles with Superior Water-Dispersibility for Photocatalysis. *Materials* **2017**, *10* (5), 566 DOI: 10.3390/ma10050566.
(27) Mowbray, D. J.; Martinez, J. I.; García Lastra, J. M.; Thygesen, K. S.; Jacobsen, K. W. Stability and Electronic Properties of TiO_2 Nanostructures with and without B and N Doping. *J. Phys. Chem. C* **2009**, *113* (28), 12301−12308.
(28) Mosier, A. R.; Guenzi, W. D.; Miller, L. L. Photochemical Decomposition of DDT by a Free-Radical Mechanism. *Science* **1969**, *164* (3883), 1083−1085.
(29) Dang, M.; Chen, D.; Lu, P.; Xu, G. Enhanced degradation of DDT using a novel iron-assisted hydrochar catalyst combined with peroxymonosulfate: Experiment and mechanism analysis. *Chemosphere* **2022**, *307* (Part 4), No. 135893, DOI: 10.1016/j.chemosphere.2022.135893.

https://doi.org/10.1021/acsomega.3c08050
ACS Omega 2024, 9, 7976−7985